Supplementary Information: Ultrafast Nuclear Dynamics of the Acetylene Cation $C_2H_2^+$ and its Impact on the Infrared Probe Pulse Induced C-H Bond Breaking Efficiency

Nadja Hartmann,*[a] Swarnendu Bhattacharyya, [b] Fabian Schlaepfer, [a] Mikhail Volkov, [a] Zeno Schumacher, [a] Matteo Lucchini, [c] Lukas Gallmann, [a] Ursula Rothlisberger [b] and Ursula Keller [a]

Experimental Methods

The experiments were performed using the extreme-ultraviolet (XUV)-pump/infrared (IR)-probe setup[1] shown in figure 1a of the main text. A 30 fs IR laser pulse at a central wavelength of 780 nm from a commercial Ti:sapphire system with a 1-kHz pulse repetition rate was spectrally broadened via filamentation[2] in argon and subsequently compressed with a pair of chirped mirrors. Thereafter, the beam was split in a 80:20 ratio using a beam splitter (BS). The more energetic part of the beam was used for high-harmonic generation (HHG) in xenon, yielding an XUV attosecond pulse train (APT) spectrally extending from 20 to 35 eV. The residual IR radiation was subsequently blocked using a 100-nm thick aluminum (Al) filter. The spectrum of the XUV pulse could optionally be filtered to contain mainly one dominant harmonic around 23.5 eV using an additional 100-nm thick tin (Sn) foil. The second part of the IR beam was guided via a piezoelectric delay stage and could be varied in peak-intensity from 1 to 5 $\cdot 10^{12}$ W cm-2 using a motorized iris. Both beams were recombined using a center-hole mirror and focused into the interaction region in front of a time-of-flight (TOF) spectrometer. The cross-correlation of the pump and probe pulses was obtained by ionizing argon as described below and the full-width at half maximum (FWHM) was found to be 15 $\pm$ 2 fs. From this, the XUV pump and IR probe pulse durations were estimated to be 7 and 13 fs, respectively, as described in more detail in the next section. After the interaction region the IR was blocked with a second aluminum filter of 200-nm thickness and the transmitted XUV was recorded on a spectrometer. Gaseous acetylene was introduced into the interaction region through a stainless steel nozzle with an opening of 133 μm in diameter. The molecule was buffered with helium in a ratio of 1:20 in a homebuilt gas mixing setup to avoid cluster formation. This gas mixture was excited by the XUV pump pulse and probed at variable delays using the IR probe pulse. The peak intensity of the IR pulse used for the measurement presented in figure 2b of the main text was calculated to be approximately $1.6 \cdot 10^{12}$ W cm-2. At this intensity the IR pulse alone was found to be insufficient to ionize the target gas on its own. The ion fragments resulting from the pump-probe interaction were detected with the TOF spectrometer. A tuning fork chopper swinging at 500 Hz was placed in the probe arm of the experimental setup and blocked every second IR probe pulse. To improve the signal-to-noise ratio, the experiment was referenced shot-to-shot, enabling a direct subtraction of the XUV induced static ionization yield[3]. From two consecutive shots the delay-dependent relative change of the fragment ion yield $I_{Rel}(\tau) = \frac{I_{XUVIR}(\tau) - I_{XUVonly}}{\langle I_{XUVonly} \rangle}$ was extracted.

Data Processing

The averaged relative change of the fragment ion yields shown in figure 2b of the main text were computed from six individual XUV-pump/IR-probe delay scans. We defined positive delays as the IR pulse reaching the gas target after the XUV pulse. Each scan consists of a series of pairs of TOF spectra acquired over a delay window of 140 fs with steps of 2 fs between consecutive acquisitions. For each TOF spectrum, the measured signal intensity in a mass-over-charge window of 0.2 u/e around peaks corresponding to specifically chosen fragment ions was integrated to obtain the respective delay-dependent yields. Zero delay, defined as the maximum overlap of pump and probe pulses, was determined using the reconstruction of attosecond beating by interference of two-photon transitions (RABBITT)[4] technique in argon as described below. Further, the fragment ion traces were fitted using an exponentially modified Gaussian (EMG) function f_{EMG}, , multiplied with a term describing two damped oscillations, f_{Osc}, as described in detail by Trushin et al.[5]. The full fitting function is then given by $f_{Fit} = f_{EMG} \cdot f_{Osc}$. The variance σ^2 and the time zero t_0 of the EMG functions were fixed to the values extracted from the RABBITT measurements, while the decay times τ_{EMG}, τ_1 and τ_2, the oscillation frequencies ω_1 and ω_2, the phases φ_1 and φ_2 and the amplitudes A, B and C were free fitting parameters. Least squares optimization yielded oscillation periods of 65 ± 12 fs and 20 ± 2 fs for the molecular ion C2H2+ yield and 66 ± 11 fs and 20 ± 2 fs for the dehydrogenated ion C2H+ yield. The errors correspond to the standard deviation over three individual series of six scans each. The values extracted from the fits are within errors in agreement with the oscillation periods stated in the main text found using a Fourier analysis.

$$f_{EMG}(t) = A \cdot \exp\left(\frac{2t_0 + \sigma^2/\tau_{EMG} - 2t}{2\tau_{EMG}}\right) \cdot erfc\left(\frac{t_0 + \sigma^2/\tau_{EMG} - t}{\sqrt{2}\sigma}\right)$$

$$f_{Osc}(t) = 1 + B \cdot cos\big(\omega_1(t - t_0) - \varphi_1\big)e^{-\frac{t}{\tau_1}} + C \cdot cos\big(\omega_2(t - t_0) - \varphi_2\big)e^{-\frac{t}{\tau_2}}$$

RABBITT

We used the RABBITT[4] technique to characterize the XUV pump and IR probe pulses and to find zero delay, defined as the moment of maximum temporal overlap of the two pulses. Photoionization of argon with an APT from HHG leads to distinct peaks in the photoelectron spectrum corresponding to the individual harmonics constituting the spectrum of the APT. When an additional time delayed IR pulse at the fundamental frequency is added, the photo electrons emitted by the XUV pulse can undergo a further transition by either absorbing or emitting one IR photon. Since the harmonics of the APT are energetically separated by two times the energy of the fundamental, these two pathways through neighboring harmonics can lead to the same final energy and produce side bands (SB). Fitting these signals allow the extraction of the time of maximum overlap and the cross correlation of the XUV and IR pulses. The envelope of the side band signal corresponds to the convolution of the envelopes of the APT and the IR pulse and was fitted using a Gaussian function. Its peak was then defined as zero delay for the subsequent scans performed in acetylene. As a rule of thumb, the duration of the envelope of

[a] *Department of Physics, ETH Zurich, 8093 Zurich, Switzerland.*
[b] *Laboratory of Computational Chemistry and Biochemistry, EPFL, 1015 Lausanne, Switzerland.*
[c] *Physics Department, Politecnico di Milano, 20133 Milan, Italy.*
Electronic Supplementary Information (ESI) available: SupplementaryInfo.pdf containing further descriptions of the experimental and theoretical methods used. See DOI: 10.1039/x0xx00000x

the APT can be assumed to be roughly half that of the IR pulse. Further, assuming Gaussian envelopes for both pulses allows to calculate the individual full width at half maximum durations stated in the main text.

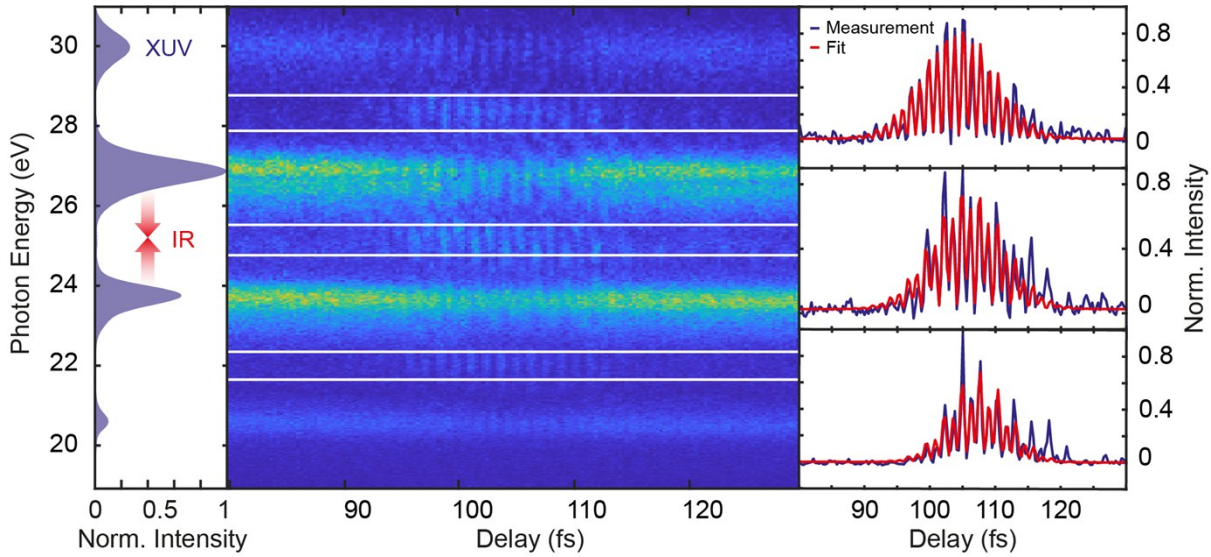

Figure S1 Photoionization of argon using an APT results in distinct peaks in the photoelectron spectrum corresponding to the individual high harmonics shown in the left panel. These peaks form the main bands in the photoelectron spectrum shown in the central panel. The addition of an IR beam at the fundamental frequency of the HHG process leads to the formation of side bands (SB) due to absorption or stimulated emission of one IR photon by the photoelectron. Due to quantum path interferences the SB signal oscillates as a function of the pump-probe delay at twice the fundamental frequency and can be fitted to extract the maximum temporal overlap of the XUV and IR pulses and their cross correlation.

Additional comparisons

The dependence of the features observed in the change of the fragment yields on the pump and probe pulse parameters was investigated by comparing measurements taken with different IR intensities (figure S2a) and different XUV spectra (figure S2b). Neither increasing the probe pulse intensity nor adding a tin filter to suppress the XUV spectrum above 25 eV, while keeping the IR pulse length constant, affected the experimental observations qualitatively. However, the amplitude of the modulations of the C-H bond breaking efficiency leading to C_2H^+ formation shows a slight increase as a function of the IR intensity. Additionally, the ratio of the peaks located at delay zero and 60 fs changes with increasing IR intensity. While at the lowest intensity the peak at the pump-probe overlap is clearly stronger than the one appearing at 60 fs, their intensities are almost equal for the largest shown IR intensity. This can be seen directly in figure S3, where the ratio of the maxima located around time zero and 60 fs respectively is shown for the different IR peak intensities used. Since different pathways are expected to scale differently with increasing IR intensity, our observation indicates that the two peaks arise due to different mechanisms or a different mixture of mechanisms being accessible to the electronic wave packet at this particular pump-probe delay. Furthermore, high IR fields may result in a transient deformation of the potential energy surfaces. This can cause an IR-dependent modification of the transition probabilities and/or branching ratios and thus affect the relative contributions of the discussed mechanisms. The insensitivity to a restriction of the XUV spectrum to below 25 eV confirms the assumption that even with the full spectrum the energetically higher lying states are populated only sparsely due to their very small photoionization cross-section. These states thus do not influence the observed fragmentation dynamics. It is important to note that both XUV spectra, the filtered and the unfiltered, do not contain photons that are energetic enough to cause double ionization. It follows that the observed dynamical behavior is connected to the evolution of the energetically lower lying states.

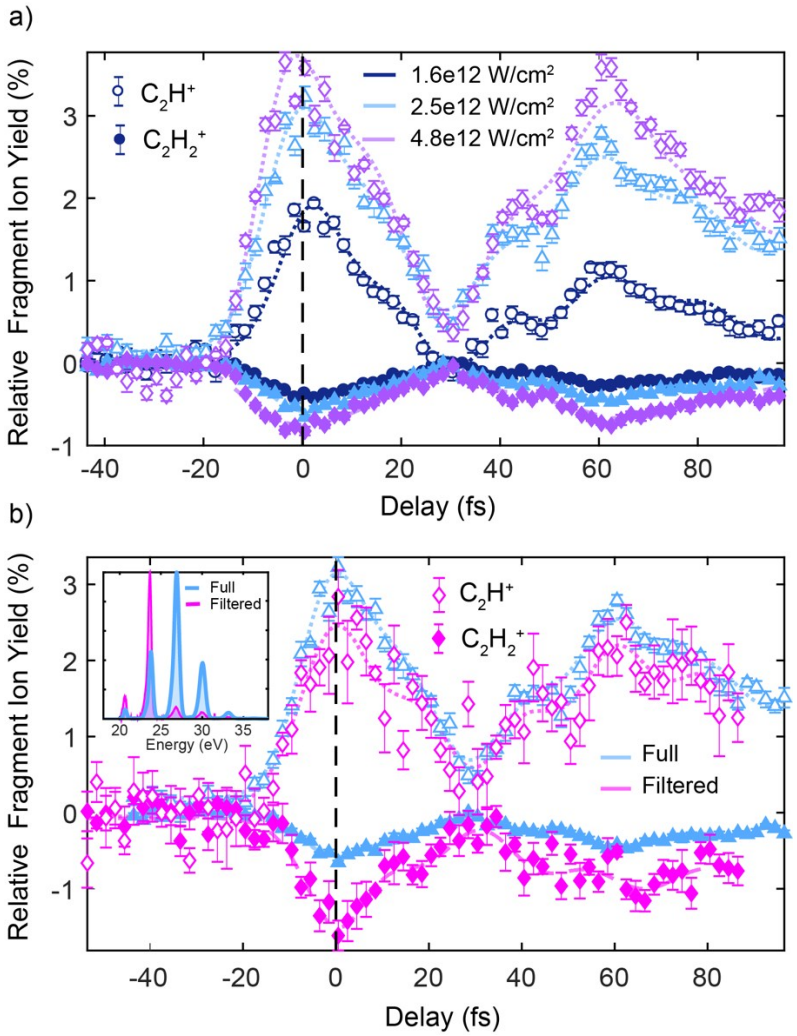

Figure S2 Experimental data for varying pulse parameters. a) The dynamics of the fragment ion yields does not depend on the IR peak intensity, but the amplitude increases with the pulse energy. b) No significant changes in the fragment yield dynamics are observed when a 100 nm thick Sn foil is introduced to reduce the XUV spectrum to a single harmonic around 23.5 eV.

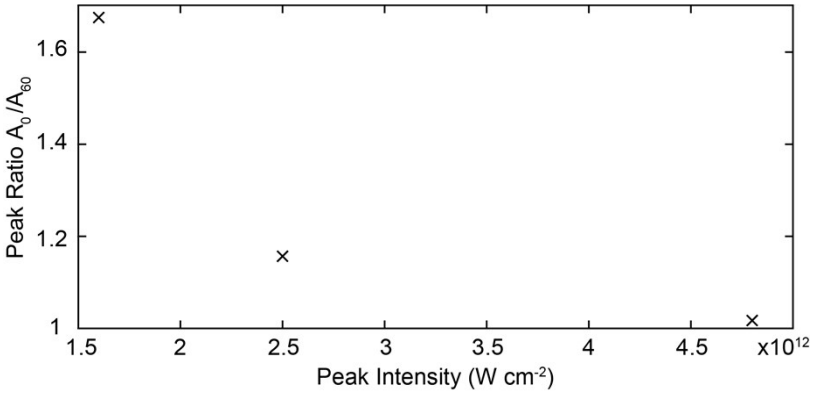

Figure S3 The ratio of the peaks observed in the C_2H^+ ion yield around time zero and 60 fs after pump probe overlap plotted as a function of the IR peak intensity used.

Static electronic structure calculations

Several cuts of the potential-energy surfaces (PESs) of the ground and the first few excited electronic states of the acetylene cation have been constructed along the dynamically significant vibrational modes. The extended multi-state complete active space second-order perturbation theory (XMS-CASPT2) method has been employed in all the single point electronic energy calculations to take into account the so-called dynamic electron-correlation effects[6]. The reference wave function for the XMS-CASPT2 calculations has been obtained from a preceding state-averaged complete active space self-consistent field (SA-CASSCF) calculation. All the electronic states have been given equal weight in the state averaging process of the CASSCF calculations. A full-valence (9,10) active space has been employed to achieve a balanced description of the ground and the excited-state electronic wave functions at a large variety of nuclear configurations. Dunning's correlation-consistent triple-**ζ** basis set (cc-pVTZ) has been used throughout[7]. Molecular point-group symmetries have been exploited wherever possible. The MOLPRO quantum chemistry package was used for all the single point calculations[8, 9]. The ground state equilibrium geometry of the neutral acetylene has been optimized at the CCSD(T)/cc-pV5Z level and the optimized values of the C-H and the C-C bond lengths are 1.06304 Å and 1.20574 Å, respectively. The value of the first ionization potential (IP) has been computed to be 11.48 eV at the RCCSD(T)/aug-cc-pV5Z level. This is in good agreement with the experimental value of 11.49 eV obtained from a high-resolution photoelectron spectroscopy experiment[10].

Up to 16 electronic states were included in the electronic structure calculations along the C-H (figure 1c) and C-C (figure S3a) bond stretching and C-C-H bending (figure S3b) coordinates to investigate the behavior of the dense manifold of higher lying states upon large distortions. The PES scans are static, meaning that all the nuclear coordinates except the one under consideration are kept frozen at their molecular ground state equilibrium value. The electronic states have been labeled according to the symmetry group conserved during the motion along the coordinate of the PES cuts. A comparison of figures 1c and S4a reveals that, upon preparation of the system in the first excited state, the C-C dissociation asymptote exhibits a much larger energy barrier than the C-H dissociation asymptote. This could explain, why no C-C dissociation has been observed in the FSSH simulations.

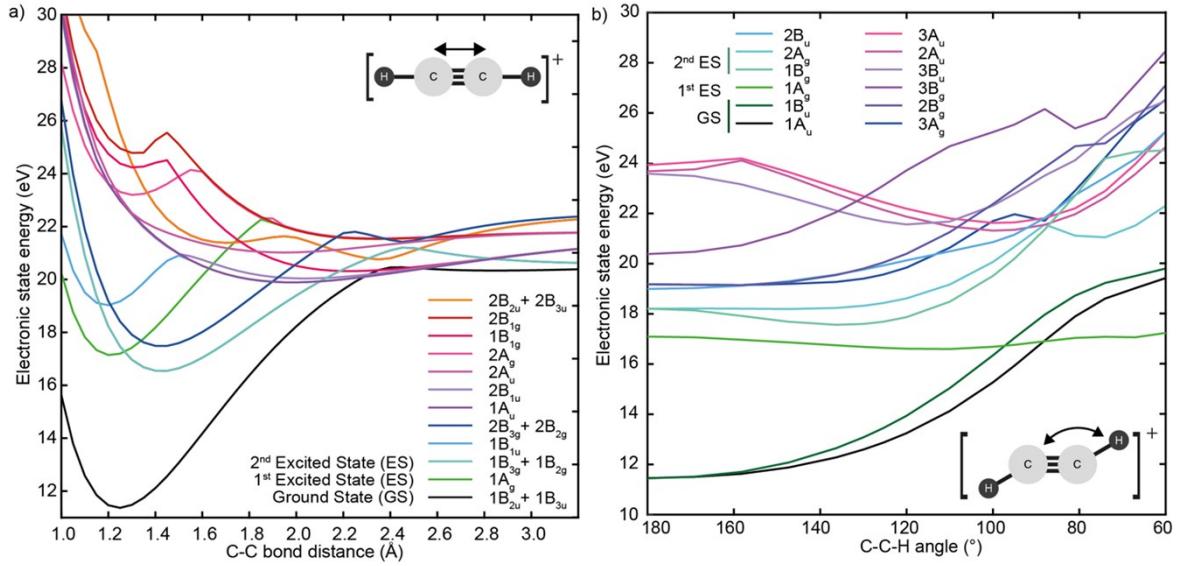

Figure S4 The 16 respectively 12 lowest electronic states of the acetylene cation $C_2H_2^+$ as a function of a) the single C-C bond stretching coordinate and b) the C-C-H trans-bending angle, calculated at the XMS-CASPT2/CASSCF/cc-pVTZ level.

Non-adiabatic dynamics simulation with trajectory surface hopping

Non-adiabatic dynamics simulations have been carried out to investigate the population dynamics of the excited states of the acetylene cation following the photo-ionization event. We assume ionization from the HOMO-1 ($^{3}\sigma_{g}$) orbital, which creates the cation in the $^{\Sigma}{}_{g}^{+}$ state. The five energetically lowest electronic states have been considered. Tully's fewest switches surface hopping (FSSH) method[11, 12] has been employed, where the PESs, the energy-gradients and the non-adiabatic couplings have been calculated on-the-fly. All dynamic simulations have been performed at the SA(5)-CASSCF level with a (9,8) active space using a 6-31G** basis set. The non-adiabatic couplings between the force state and all the other (four) states have been calculated at each time step. Within the FSSH method, the quantum nuclear wave packet is approximated as a set of points in phase space, which are propagated independently in time following Newton's equation of motion. The classical trajectories may hop from one electronic state to another upon fulfilment of a stochastic hopping criterion. We sampled 80 initial conditions from the Wigner distribution of the vibrational ground state in the electronic ground state of the neutral acetylene molecule at 100 K. The initial conditions have been propagated up to 200 fs, where the Newton's equation of motion has been integrated with 0.1 fs time steps. The coefficients associated with the different adiabatic electronic states have been determined by solving the time-dependent Schrödinger equation, which has been integrated in intervals of 0.001 fs. All the FSSH dynamics simulations have been performed with Newton-X[13, 14], using the Columbus quantum chemistry package[15] for the underlying electronic structure calculations. The time-dependent population of the lowest five electronic states up to 200 fs is shown in figure 3 of the main text. Since, the dynamics is performed in the adiabatic electronic representation, the D_i state describes the i^{th} energy ordered state at any instant of time. As discussed in the main text, the results show a fast population transfer from the initially populated D_2 to the D_3 and D_4 states. This is due to a small energy gap and a non-negligible non-adiabatic coupling between them. Further, a major non-adiabatic transition from the D_2 to the D_1 and finally to the D_0 state occurs between 25 and 50 fs. After 50 fs the population decay slows down and the dynamics is dominated by a steady transfer from the D_2 to the D_0 state, keeping the population of the intermediate D_1 state in a dynamic equilibrium. The observed oscillations of the C-C bond length (figure S5a) and the molecular trans-bending motion (figure S5b) are in agreement with previous non-adiabatic studies[16].

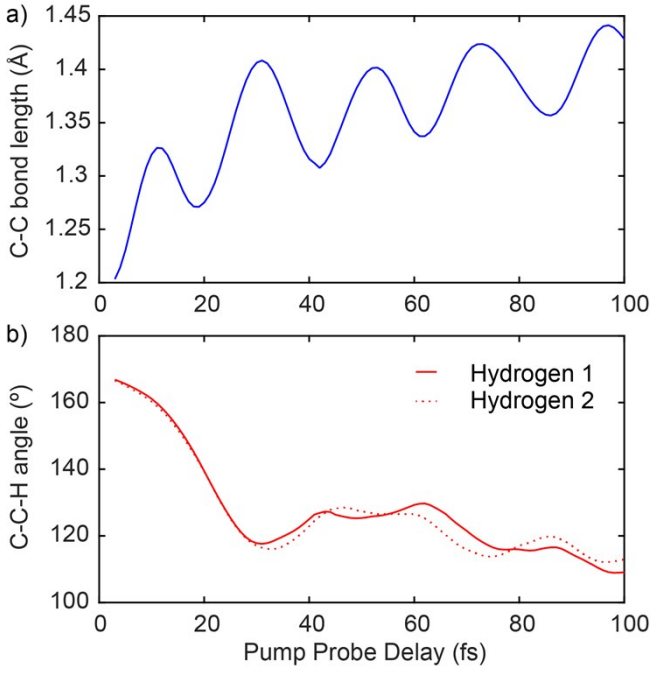

Figure S5 The evolution of a) the C-C bond length and b) the C-C-H trans-bending angles for both sides of the acetylene molecule averaged over all 80 trajectories started on the D2 state.

Besides the well-known isomerization through CI, non-adiabatic dynamics simulations have exhibited direct C-H dissociations as well. Such a dissociating trajectory is shown in figure 4e in the main text. A careful analysis of the FSSH data have provided us with two possible mechanisms for the action of the IR probe pulse in mediating the fragmentation ion yields. For the figures shown in the main manuscript, we have chosen two trajectories from our simulations to demonstrate the respective mechanisms. One of them exhibits C-H dissociation while the other does not. The excitation at small delays and the dumping around 30 fs after excitation has been discussed in the main text. Here, we want to show the re-excitation mechanism mentioned in the main text. Similar as in the main text, we observe a non-dissociating trajectory (figure S6a). The analysis of the energy gaps between the D_0 state and the D_2 and D_3 states with time reveals that they may become resonant with the IR photon energy (figure S6b). Therefore, absorption of one photon at this time can promote the relaxed system from the ground state to excited states, where dissociation may occur. To demonstrate this pathway, we have promoted our trajectory from the D_0 to the D_3 state at 49.4 fs (indicated by the red arrow in figure S6c) and propagated it normally. A comparison of the variation of C-H bond lengths along the two trajectories, shown in figure S6d, clearly demonstrates the fact that absorption of one IR photon around this time can enhance C-H dissociation. This mechanism can thus contribute to the experimentally observed enhancement of the C_2H^+ yield around 60 fs.

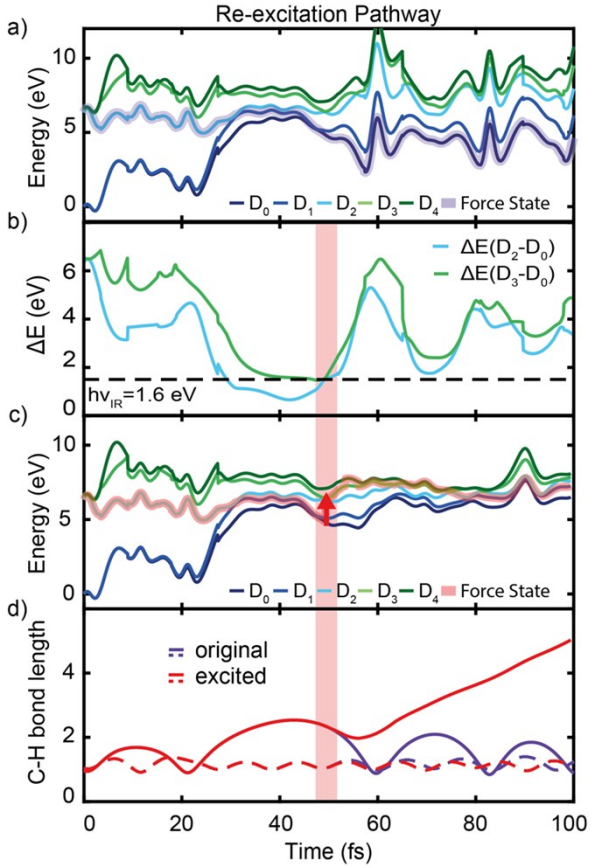

Figure S6 Demonstration of the enhancement of the fragmentation by absorption of IR radiation around 50 fs. a) Energy profile of the original trajectory, which does not exhibit any C-H dissociation. b) Corresponding energy gap from the D_0 to the D_2 and D_3 states. The IR photon energy ($h\nu_{IR} \approx 1.6$ eV) is indicated as the black dashed line. c) Energy profile of the trajectory corresponding to a promotion from the D_0 to the D_3 state at 49.4 fs, designated by the red arrow. d) Evolution of C-H bond lengths for the two C-H bonds and for both the trajectories, respectively, which reveals C-H bond dissociation in the promoted trajectory.

References

1. R. Locher, M. Lucchini, J. Herrmann, M. Sabbar, M. Weger, A. Ludwig, L. Castiglioni, M. Greif, M. Hengsberger, L. Gallmann and U. Keller, *Rev. Sci. Instrum.*, 2014, **85**, 13113.

2. A. Braun, G. Korn, X. Liu, D. Du, J. Squier and G. Mourou, *Optics Letters*, 1995, **20**, 73-75.

3. A. Ludwig, E. Liberatore, J. Herrmann, L. Kasmi, P. Lopez-Tarifa, L. Gallmann, U. Rothlisberger, U. Keller and M. Lucchini, *The Journal of Physical Chemistry Letters*, 2016, **7**, 1902-1906.

4. P. M. Paul, E. S. Toma, P. Breger, G. Mullot, F. Augé, P. Balcou, H. G. Muller and P. Agostini, *Science*, 2001, **292**, 1689-1692.

5. S. A. Trushin, K. Kosma, W. Fuß and W. E. Schmid, *Chem Phys*, 2008, **347**, 309-323.

6. T. Shiozaki, W. Győrffy, P. Celani and H.-J. Werner, *The Journal of Chemical Physics*, 2011, **135**, 081106.

7. D. E. Woon and T. H. D. Jr., *The Journal of Chemical Physics*, 1993, **98**, 1358-1371.

8. H.-J. Werner, P. J. Knowles, G. Knizia, F. R. Manby and M. Schütz, *Wiley Interdisciplinary Reviews: Computational Molecular Science*, 2012, **2**, 242-253.

9. H.-J. Werner, P. J. Knowles, G. Knizia, F. R. Manby, M. Schütz, P. Celani, W. Györffy, D. Kats, T. Korona, R. Lindh, A. Mitrushenkov, G. Rauhut, K. R. Shamasundar, T. B. Adler, R. D. Amos, A. Bernhardsson, A. Berning, D. L. Cooper, M. J. O. Deegan, A. J. Dobbyn, F. Eckert, E. Goll, C. Hampel, A. Hesselmann, G. Hetzer, T. Hrenar, G. Jansen, C. Köppl, Y. Liu, A. W. Lloyd, R. A. Mata, A. J. May, S. J. McNicholas, W. Meyer, M. E. Mura, A. Nicklass, D. P. O'Neill, P. Palmieri, D. Peng, K. Pfl\"uger, R. Pitzer, M. Reiher, T. Shiozaki, H. Stoll, A. J. Stone, R. Tarroni, T. Thorsteinsson and M. Wang, MOLPRO, version 2015.1, a package of ab initio programs, http://www.molpro.net).

10. G. Bieri and L. Åsbrink, *Journal of Electron Spectroscopy and Related Phenomena*, 1980, **20**, 149-167.

11. J. C. Tully, *Faraday Discussions*, 1998, **110**, 407-419.

12. J. C. Tully, *J. Chem. Phys.*, 1990, **93**, 1061.

13. M. Barbatti, M. Ruckenbauer, F. Plasser, J. Pittner, G. Granucci, M. Persico and H. Lischka, *WIREs: Comp. Mol. Sci.*, 2014, **4**, 26-33.

14. M. Barbatti, G. Granucci, M. Ruckenbauer, F. Plasser, R. Crespo-Otero, J. Pittner, M. Persico and H. Lischka, NEWTON-X: A package for Newtonian dynamics close to the crossing seam. Version 2, www.newtonx.org).

15. H. Lischka, R. Shepard, I. Shavitt, R. M. Pitzer, M. Dallos, T. Müller, P. G. Szalay, F. B. Brown, R. Ahlrichs, H. J. Böhm, A. Chang, D. C. Comeau, R. Gdanitz, H. Dachsel, C. Ehrhardt, M. Ernzerhof, P. Höchtl, S. Irle, G. Kedziora, T. Kovar, V. Parasuk, M. J. M. Pepper, P. Scharf, H. Schiffer, M. Schindler, M. Schüler, M. Seth, E. A. Stahlberg, J.-G. Zhao, S. Yabushita, Z. Zhang, M. Barbatti, S. Matsika, M. Schuurmann, D. R. Yarkony, S. R. Brozell, E. V. Beck, J.-P. Blaudeau, M. Ruckenbauer, B. Sellner, F. Plasser, J. J. Szymczak and R. F. K. Spada, A. Das. COLUMBUS , an ab initio electronic structure program, release 7.0, www.univie.ac.at/columbus.).

16. H. Ibrahim, B. Wales, S. Beaulieu, B. E. Schmidt, N. Thiré, E. P. Fowe, E. Bisson, C. T. Hebeisen, V. Wanie, M. Giguére, J.-C. Kieffer, M. Spanner, A. D. Bandrauk, J. Sanderson, M. S. Schuurman and F. Légaré, *Nat. Commun.*, 2014, **5**, 4422.